Adsorption (2011) 17: 109–120
DOI 10.1007/s10450-010-9297-z

Effect of dead volume on performance of simulated moving bed process

Young-Il Lim · Suresh K. Bhatia

Received: 11 May 2010 / Accepted: 19 November 2010 / Published online: 30 November 2010

Abstract The volume of surrounding equipments (pipe transfer lines and valves) in the simulated moving bed (SMB) unit, which is called the dead volume, is modeled as bed-head, bed-tail and bed-line. Since the dead volume can be significant especially in industrial-scale SMB units, the consideration of dead volume has been required for high performance operation. In this study, a simple and unified approach based on the method of characteristics (MOC), called the extended node model, is established to solve fluid concentration dynamics within dead volumes. The computational efficiency of the approach is evaluated for three case studies of a standard four-zone SMB process with a linear adsorption equilibrium model. Insertion of one zone to flush the fluid trapped in extract bed-line into the standard four-zone SMB improves substantially purity, while recovery is kept constant.

Keywords Simulated moving bed (SMB) · Dead volume · Mathematical modeling · Method of characteristics (MOC) · Flushing · Purity improvement

Notation

A	more retained component
B	less retained component
C	fluid concentration (g/l)
C_A	fluid concentration of component A (g/l)
C_B	fluid concentration of component B (g/l)
C_{des}	desorbent concentration (g/l)
C_{ext}	extract concentration (g/l)
C_{feed}	feed concentration (g/l)
C_{flush}	flush concentration (g/l)
C_{raf}	raffinate concentration (g/l)
D_{ax}	axial diffusion coefficient inside adsorptive bed (cm^2/min)
$D_{ax,dead}$	axial diffusion coefficient inside dead volume (cm^2/min)
k	overall mass transfer coefficient (min^{-1})
L_c	bed length (cm)
L_{dead}	length occupied by dead volume assuming the diameter is same as the bed diameter (cm)
$\dot{m}_{loss}$	mass flowrate lost through bed-line (mg/min)
n	solid concentration (g/l)
n^*	equilibrium solid concentration (g/l)
N	bed number
N_{bed}	total bed number
N_{CFL}	CFL number
N_{mesh}	number of mesh (or grid) points
N_{MOC}	number of mesh points used by MOC
N_{time}	number of time levels
Pe	Peclet number ($= v_L L_c / D_{ax}$)
Pe_{dead}	Peclet number inside dead volume
Q_{ext}	extract flowrate (ml/min)
Q_{feed}	feed flowrate (ml/min)
Q_{flush}	flush flowrate (ml/min)
Q_{raf}	raffinate flowrate (ml/min)
Q_{rec}	recycle flowrate (ml/min)
R_A	extract recovery of component A
t	time (min)
t_{lag}	lag time caused by dead volume (min)
v_{dead}	velocity inside dead volume (cm/min)

Y.-I. Lim (✉)
Department of Chemical Engineering, Hankyong National University, Gyonggi-do, Anseong-si 456-749, Korea
e-mail: limyi@hknu.ac.kr

S.K. Bhatia
Division of Chemical Engineering, The University of Queensland, Brisbane, Queensland 4072, Australia

v_L interstitial velocity inside the adsorptive bed (cm/min)
z axial distance (cm)

Greek letters

ε_b bed voidage
γ spatial length ratio
Δt time stepsize (min)
Δz spatial stepsize (cm)
Δz_{MOC} spatial stepsize used by MOC (cm)
τ switching time (or shifting time, min)

Subscripts and superscripts

hi bed-head inlet
hm bed-head index crossed by the characteristics line at the previous time level
ho bed-head outlet
i component index
j dead volume index (bed-head, bed-tail, or bed-line)
k bed number index
l mesh point index used by MOC
li bed-line inlet
lo bed-line outlet
n time level index
ti bed-tail inlet
tm bed-tail index crossed by the characteristics line at the previous time level
to bed-tail outlet

1 Introduction

Simulated moving bed (SMB) chromatography, a continuous multi-column chromatographic process, has emerged as a promising technology for the separation of petrochemicals, sugars, pharmaceuticals, and bio-molecules (Juza et al. 2000; Rajendran et al. 2009; Sá Gomes et al. 2006; Seidel-Morgenstern et al. 2008). SMB chromatography usually works with the inherent advantage of a high driving force due to counter-current flow, resulting in low solvent consumption, small apparatus scale and high yield, compared to batch chromatography (Lim and Jorgensen 2007; Zhang et al. 2004a). In SMB operation, the countercurrent movement of fluid and solid is simulated by an appropriate flow switching sequence, resolving problems associated with the solid circulation in the true moving bed (TMB) unit where liquid and solid flow in the opposite direction. The fixed beds of SMB are divided into several zones by inlet and outlet streams, while the inlet (e.g., desorbent and feed) and outlet ports (e.g., extract and raffinate) move simultaneously one column ahead at a given switching time interval in the direction of the fluid flow (Pais et al. 1998).

The SMB process was developed by Universal Oil Products (UOP, USA) in the 1960s (Broughton and Gerhold 1961). SMB has been successfully commercialized within the petrochemical industry (Sá Gomes et al. 2006), sugar processing industry (Beste et al. 2000; Wooley et al. 1998; Xie et al. 2005) and more recently within the area of chiral separations (Juza et al. 2000; Rajendran et al. 2009). Various approaches have been taken to reduce the production cost and improve the separation efficiency of the SMB processes by operating SMB under more complex dynamic conditions, as the case in Varicol (Ludemann-Hombourger et al. 2000, 2002), PowerFeed (Kearney and Hieb 1992; Zhang et al. 2004a, 2004b), ModiCon (Schramm et al. 2003), and Partial-Discard (Bae and Lee 2006). These new operation modes do not keep constant conditions during one switching period, as in a standard SMB, but allow for variation of the column configuration, the feed flowrates, the feed concentration, and the withdrawal time of products, respectively. Classical four-zone SMB was only capable of separating binary mixtures or dividing multi-component mixtures into strong adsorbing and weak adsorbing fractions (Wang and Ching 2005), while five-zone (Nicolaos et al. 2001a, 2001b; Wang and Ching 2005; Xie et al. 2005) and nine-zone (Wooley et al. 1998) SMB processes were presented for multi-component separations of more than three components.

With the intensive and practical applications of SMB, systematic approaches have been developed for the design and optimization of SMB processes. The triangle theory under the assumption of equilibrium adsorption and TMB was developed for linear and nonlinear adsorption isotherms with successful applications (Gentilini et al. 1998; Katsuo et al. 2009; Mazzotti et al. 1997). As an another theoretical approach, the standing wave analysis provided an analytical solution of SMB zone flowrates at steady-state under the TMB assumption for equilibrium and nonequilibrium adsorptions without and with mass transfer resistance, respectively (Hritzko et al. 2002; Ma and Wang 1997; Mallmann et al. 1998). Apart from the TMB assumption for the theoretical analyses, the SMB model representing realistic port switching by the node model was able to consider periodic dynamics of the SMB operation (Beste et al. 2000; Lim and Jorgensen 2004; Ma and Wang 1997; Pais et al. 1998).

More sophisticated designs and operations in the production scale have been required for complex mixtures, desired purity and higher productivity with the increasing demand in petrochemical, pharmaceutical and food industries. A large-scale SMB process with five-zones was reported for six-sugar separation from biomass hydrolyzate (Xie et al. 2005). A production-scale SMB process with five zones of 20 columns was presented for valuable protein separation from whey protein concentrate (Andersson and Mattiasson 2006). The Parex unit for p-xylene separation from its C_8 aromatic isomers (m-xylene, o-xylene, and ethylbenzene)

was composed of a seven-zone SMB to increase the purity by flushing bed-lines contaminated by impurities (Minceva and Rodrigues 2003). The dead volume (e.g., extra-column dead volume and bed-line) had to be properly accounted for in these practical applications (Lim et al. 2010; Rajendran et al. 2009). Even in a small-scale high pressure liquid chromatography (HPLC) SMB unit for racemic mixture separation, the dead volume of connecting tubing parts and valves was comparable to the column volume (Katsuo et al. 2009; Sá Gomes et al. 2010).

A simple way for the consideration of dead volume was to use an effective bed length and effective bed voidage (Beste et al. 2000; Lim and Jorgensen 2007). The effect of extra-column dead volume on SMB performance was theoretically analyzed in the framework of both the triangle theory (Migliorini et al. 1999) and standing wave design (Mun et al. 2003) in terms of the time delay caused by the dead volume. To represent dynamics of the extra-column dead volume, a convection-diffusion model without adsorption was used, which was solved together with the adsorptive partial differential equation (PDE) model by an implicit time integrator after spatial discretization (Jin and Wankat 2007; Katsuo et al. 2009; Zabka et al. 2008). Since the bed-line dead volume trapped in the transfer line had a temporally discontinuous feature different from the extra-column dead volume, the dynamics caused by the bed-line were numerically treated, distinguishing three different stages like time events during one switching period, by using an explicit time integrator (Minceva and Rodrigues 2003).

However, it may not be necessary to solve a non-adsorption PDE model together with the adsorption PDE for the consideration of dead volume dynamics (Lim et al. 2010). Furthermore, for an implicit time integrator (e.g., Gear method) commonly used for solving the SMB model (Kurup et al. 2005), it is not trivial to treat the time events caused by the bed-line. The fluid concentration dynamics of dead volume were solved for an industrial-scale para-xylene SMB process by using an extended node model with the method of characteristics (MOC) in the framework of the unified dead volume treatment for bed-head, bed-tail, and bed-line (Lim et al. 2010).

However, the performance of the novel model with MOC (Lim et al. 2010) has not been tested with a standard SMB process. In this study, the detailed numerical algorithm of this unified dead volume treatment approach is described. The computational efficiency of the model is evaluated for a standard 4-zone SMB unit with a linear adsorption equilibrium model. The internal and external fluid concentration profiles according to the dead volumes (bed-head, bed-tail and bed-line) are obtained from the extended node model with MOC. The effects of the dead volumes are investigated on process performance in terms of purity and recovery. This study reinforces theoretical backgrounds of our unified dead volume treatment approach previously applied to an industrial para-xylene SMB process.

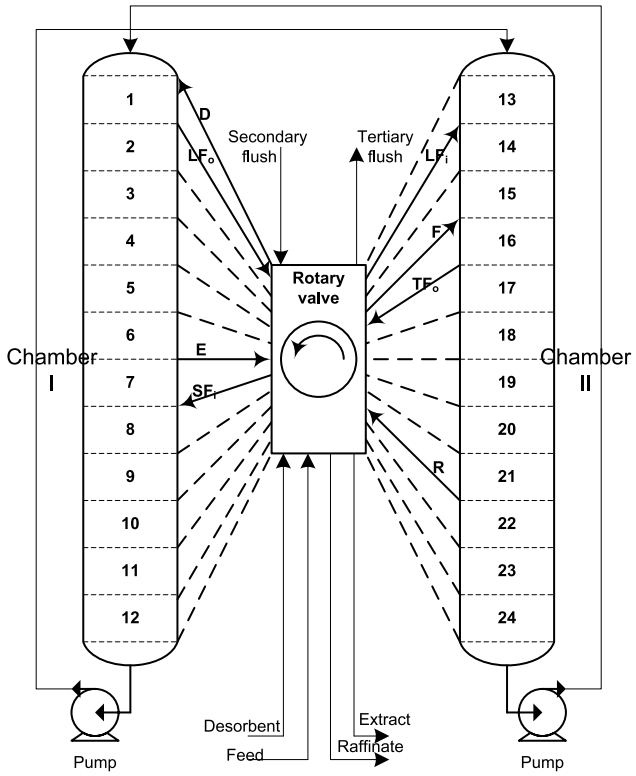

Fig. 1 Schematic diagram of Parex SMB process (Lim et al. 2010)

2 Dead volume and extended node model

Dead volumes are always present due to tubes, valves, and pumps and may account for up to 3% of the unit volume in industrial- or pilot-scale SMB plants (Jin and Wankat 2007). Two types of the dead volume: extra-column dead volume (Katsuo et al. 2009; Migliorini et al. 1999) and bed-line (Lim et al. 2010; Minceva and Rodrigues 2003) were reported. The eight-zone Parex SMB unit for p-xylene separation (Lim et al. 2010) is illustrated to identify these dead volumes in the industrial-scale process in Fig. 1. Each bed is connected to a flow directing device, known as a rotary valve, by a bed-line. A pump provides the liquid circulation from the bottom of the chamber to the top. The port switching is realized by the rotation of the unique rotary valve. Every line connecting the rotary valve to adsorbent beds is shared by inlet and outlet streams (desorbent, feed, extract and raffinate). For illustration, the same bed-line is used for introducing the feed into the unit and later for withdrawing the extract from the unit (Lim et al. 2010; Minceva and Rodrigues 2003). Therefore, the bed-lines should be contaminated by other inlet or outlet streams, resulting in reduced product purity, otherwise an appropriate

action is taken. In order to prevent the extract stream from being contaminated by xylene isomers and to increase recovery, the Parex unit has internal line flushing (LF_i) and external flushing (LF_o) sequences added to conventional four-zone SMB port switching (Frey 2007; Lim et al. 2010; Noe 1999; Wei 1998), which makes the total number of zones seven or eight. In Fig. 1, an additional dead volume is observed, connecting the bottom of the adsorbent chamber to the top through the pump (i.e., pipe line of the recycle flow), which may exist in any inter- and intra-bed.

In this study, the dead volume in the inter- and intra-bed is conceptualized by the bed-head and bed-tail, which was called the extra-column dead volume in the literatures (Katsuo et al. 2009; Migliorini et al. 1999). The external connecting line to the bed (e.g, rotary valve to bed) was called the bed-line (Lim et al. 2010). The Nth dead volume consists of the Nth bed-head, the Nth bed-tail, and the Nth bed-line, which are all non-adsorptive regions. The bed-head corresponds to all the volume of valves and tubing parts connecting the port to the bed, a distribution plate space and other physically occupied volumes on the top of the adsorptive bed. The bed-tail contains mainly the volume of tubing parts connecting the bed end to the port. The bed-line includes the volume introducing the inlet (e.g., desorbent and feed) or outlet (e.g., extract and raffinate) stream (Lim et al. 2010).

The conventional node model representing the port (or physically the valve) between two beds has been described for inlet and outlet streams according to the port switching without considering the dead volume (Beste et al. 2000; Lim and Jorgensen 2004, 2007; Ma and Wang 1997; Pais et al. 1998). The bed-head and bed-tail (or extra-column dead volume) were treated as a part of the bed, and a convection-diffusion model was solved (Jin and Wankat 2007; Katsuo et al. 2009; Migliorini et al. 1999; Sá Gomes et al. 2010):

$$\frac{\partial C_i}{\partial t} + v_{dead}\frac{\partial C_i}{\partial z} = D_{ax,dead,i}\frac{\partial^2 C_i}{\partial z^2} \tag{1}$$

where v_{dead} is the superficial velocity of the fluid and $D_{ax,dead}$ is the axial dispersion coefficient of each component (i) in the bed-head, bed-tail or bed-line. The convection-diffusion model inside dead volume is completed with inlet and outlet boundary conditions commonly used (Beste et al. 2000; Kurup et al. 2005; Lim et al. 2010; Lim 2008; Lim and Jorgensen 2004, 2007; Minceva and Rodrigues 2003; Pais et al. 1998):

$$v_{dead}\left(C_{i,z=0} - C_{i,in}\right) = D_{ax,dead}\left.\frac{dC_i}{dz}\right|_{z=0}, \quad \forall t \tag{2}$$

$$\left.\frac{dC_i}{dz}\right|_{z=L_{dead}} = 0, \quad \forall t \tag{3}$$

where $C_{i,in}$ is the inlet concentration entering a dead volume and L_{dead} denotes the end of dead volume. The adsorption bed is modeled by a convection-diffusion-reaction PDE with linear deriving force assumption (Beste et al. 2000; Kurup et al. 2005; Lim et al. 2010; Lim and Jorgensen 2004; Ma and Wang 1997; Minceva and Rodrigues 2003; Pais et al. 1998; Sá Gomes et al. 2010):

$$\frac{\partial C_i}{\partial t} + v_L\frac{\partial (C_i)}{\partial z} = D_{ax}\frac{\partial^2 C_i}{\partial z^2} - \frac{1-\varepsilon_b}{\varepsilon_b}k_i(n_i^* - n_i) \tag{4}$$

$$\frac{dn_i}{dt} = k_i(n_i^* - n_i) \tag{5}$$

where v_L is the interstitial velocity assumed to be constant within the bed, D_{ax} is the axial dispersion coefficient, ε_b is the bed voidage, and k_i is the mass transfer coefficient for each component (i). The liquid and solid concentrations are C_i and n_i, respectively. n_i^* is an adsorption isotherms. Therefore two different PDEs (adsorption bed model and non-adsorption bed model) are solved simultaneously and the computational time proportionally increases with the dead volume. It may be more complicated to solve the bed line showing a discontinuous feature with time. Even though the bed-line model is the same as (1), this equation should be solved only for the bed-line being used at the actual time (Lim et al. 2010).

Equation (1) can be treated separately with the adsorption PDE model (4)–(5). The convection-diffusion equation has been solved very accurately by the method of characteristics (MOC) (Bruneau et al. 1997; Douglas and Russell 1982). When the node model is extended to a port switching model involving the streams of the bed-head, bed-tail and bed-line, the extended node model is able to calculate both time delays of dead volume concentrations by MOC, and flowrates and concentrations by mass conservation (Lim et al. 2010). The novel approach makes it possible to separate the adsorption bed model from the dead volume model and to exactly solve the dead volume model, (1), in a computationally efficient manner. The adsorptive bed model is solved by using any type of time integrators, and the MOC results obtained from the three types of dead volume provide the adsorption PDE model with boundary values.

3 Calculation method based on MOC

The numerical solution of (1)–(3) is expressed as the finite difference approximation combined with the method of characteristics (Bruneau et al. 1997):

$$C_{i,1}^n = C_{i,in}^n + \frac{D_{ax,dead}}{v_{dead}}\frac{C_{i,1} - C_{i,in}}{\Delta z} \tag{6}$$

$$C_{i,l}^n - \frac{D_{ax,dead,i}\Delta t}{\Delta z^2}(C_{i,l-1}^n - 2C_{i,l}^n + C_{i,l+1}^n) = \tilde{C}_{i,l}^n$$
$$l = 2, \ldots, N_{MOC} \tag{7}$$

$$C^n_{i,N_{MOC}+1} = C^n_{i,N_{MOC}} \tag{8}$$

where the subscript l and superscript n denote the spatial and temporal mesh indexes, Δz and Δt are the uniform spatial and temporal step sizes, and N_{MOC} is the number of mesh points within dead volume. $\tilde{C}^n_{i,l}$ is the value interpolated from the known values ($C^{n-1}_{i,l}$) at the previous time level ($t^{n-1} = (n-1)\Delta t$) using MOC. The first-order spatial differential term of (2) is discretized by an upwind scheme.

3.1 MOC approximation

The MOC solution ($\tilde{C}^n_{i,l}$) represents that an initial condition ($C_{i,0}(z)$ at $t = 0$) moves along a characteristics line ($z = z_0 - v_{dead}t$).

$$\tilde{C}_i(z,t) = C_{i,0}(z_0 - v_{dead}t) \tag{9}$$

That is, the MOC solution has the same value as the concentration of the previous time level (C^{n-1}_i) coming up along the characteristics line. The slope of the pathline is called the CFL (Courant–Friedrichs–Lewy) number (Mattheij et al. 2005):

$$N_{CFL,dead} \equiv v_{dead}\frac{\Delta t}{\Delta z} \tag{10}$$

For solving the convection-dominated PDEs, the time stepsize (Δt) and the spatial stepsize (Δz) have a following constraint called the CFL (Courant–Friedrichs–Lewy) condition for a positive fluid velocity (Mattheij et al. 2005):

$$0 < N_{CFL,dead} \equiv v_{dead}\frac{\Delta t}{\Delta z} \le 1.0 \tag{11}$$

At a given CFL number satisfying the CFL condition, the MOC stepsize (Δz_{MOC}) is determined as:

$$\Delta z_{MOC} = v_{dead}\frac{\Delta t}{N_{CFL,dead}} \tag{12}$$

The MOC approximation solution ($\tilde{C}^n_{i,j,k,l}$) is obtained for a component (i), a dead volume type (j = bed-head, bed-tail, and bed-line), a bed ($k = 1, 2, \ldots, N_{bed}$), and a spatial mesh point ($l = 2, 3, \ldots, N_{MOC}$).

$$\tilde{C}^n_{i,j,k,l} = \frac{C^{n-1}_{i,j,k,l-1}\cdot(\Delta z_{MOC,j,k} - z_{MOC,j,k}) + C^{n-1}_{i,j,k,l}\cdot z_{MOC,j,k}}{\Delta z_{MOC,j,k}}$$
$$l = 2, \ldots, N_{MOC,j,k} \tag{13}$$

where $\tilde{C}^n_{i,j,k,l}$ is approximated by the lever rule which is simple and exact for linear profiles and the spatial position crossed by the MOC pathline ($z_{MOC,j,k}$) at the previous time level is given:

$$z_{MOC,j,k} = \Delta z_{MOC,j,k} - v_{dead,k}\cdot\Delta t \tag{14}$$

Equation (13) leads to a set of linear equations, resulting in a symmetric band matrix. Omitting the subscripts j and k, the matrix is expressed as follows:

$$\begin{pmatrix} 1+\gamma & -\gamma & 0 & 0 & 0 \\ -\gamma & 1+2\gamma & -\gamma & 0 & 0 \\ 0 & -\gamma & 1+2\gamma & -\gamma & 0 \\ 0 & 0 & -\gamma & 1+2\gamma & -\gamma \\ 0 & 0 & 0 & -\gamma & 1+\gamma \end{pmatrix} \times \begin{pmatrix} C^n_{i,2} \\ C^n_{i,3} \\ \cdots \\ C^n_{i,N_{MOC}-1} \\ C^n_{i,N_{MOC}} \end{pmatrix} = \begin{pmatrix} \tilde{C}^n_{i,2} \\ \tilde{C}^n_{i,3} \\ \cdots \\ \tilde{C}^n_{i,N_{MOC}-1} \\ \tilde{C}^n_{i,N_{MOC}} \end{pmatrix} \tag{15}$$

where $\gamma = \frac{D_{ax,dead,i}\Delta t}{\Delta z^2}$.

The amount of dead volume may be different from bed to bed. The number of MOC grids (N_{MOC}) should be determined to ensure the accuracy of the MOC solution. Even though the MOC results are approximated from the analytical solution of (1) without diffusion, the numerical error occurring whenever the physical domain (continuous space) is transferred into the numerical domain (discrete space) is inevitable. However, there is no truncation error occurring when the derivatives of PDEs are approximated into a finite order of accuracy.

3.2 Numerical solution methods

A fast and accurate solution tool for the chromatography and SMB model (FAST-Chrom/SMB) is constructed in this study, as shown in Table 1, using the SMB model with port switching, equilibrium or non-equilibrium adsorption, and linear or nonlinear isotherms. For each bed including the bed-head ($z_{hi} < z \le z_{ho}$) and bed-tail ($z_{ti} < z \le z_{to}$), two methods are imposed sequentially to obtain fluid concentrations (C) and solid concentrations (n). Convection-diffusion-reaction PDEs describing the adsorptive bed ($0 < z \le L_c$) are solved by using an implicit or explicit time integrator. In this study, an explicit time-space conservation element and solution element (CESE) scheme (Chang 1995; Lim et al. 2004) is used, which produces a fast and accurate solution for convection-dominated problems like the SMB PDE model due to both local and global flux conservation in space and time. The inlet BC of adsorptive bed at $z = z_{ho}$ is given by the bed-head exit obtained from MOC. The concentration propagation inside the bed-tail is calculated by MOC. The node for port switching is situated in front of the bed-head and transfers an inlet boundary value of the bed-head to MOC. This node model also contains MOC for the bed-line ($z_{li} < z \le z_{lo}$) transporting an inlet or outlet stream according to port switching. The extended node model thus

Table 1 Numerical methods applied to the SMB simulation in this study

Dead volume	Bed-head		Adsorptive bed	Bed-tail		Bed-line	
Length (z)	z_{hi}	$z_{hi} < z \leq z_{ho}$	$0 < z \leq L_c$	z_{ti}	$z_{ti} < z \leq z_{to}$	z_{li}	$z_{li} < z \leq z_{lo}$
Fluid concentration	C^n_{hi}	C^n_{ho}	Time integrator results	C^n_{ti}	C^n_{to}	C^n_{li}	C^n_{lo}
Solid concentration	0	0	Time integrator results	0	0	0	0
Calculation method	MOC		CESE scheme	MOC		MOC	

Table 2 Simulation parameters of three case studies

Design parameters			
Bed configuration	2-2-2-2 or 2-1-1-2-2	Dead volume (Case 1)	Head = 0.1625, Tail = 0.8605 cm
L_c	15 cm	Dead volume (Case 2)	Bed-line = 0.1 ml
d_c	0.46 cm	Dead volume (Case 3)	Bed-line = 0.1 ml (with flushing)
ε_b	0.63		
Operating parameters			
Q_{feed}	0.25 ml/min	C_{feed}	$A = 0.05$, $B = 0.05$ g/l
Q_{des}	0.61 ml/min	C_{des}	$A = 0.0$, $B = 0.0$ g/l
Q_{ext}	0.49 or 0.52 ml/min	C_{flush}	$A = 0.03$, $B = 0.0$ g/l
Q_{rec}	0.8 ml/min	τ	3.5 min
Q_{flush}	0.0 or 0.03 ml/min	N_{shift}	24
Model parameters			
D_{ax}	$0.005 v_L$, cm^2/min	Pe	3000
$D_{ax,dead}$	$0.005 v_{dead}$, cm^2/min	Pe_{dead}	3000
Computational parameters			
Case 1		Case 2 and 3	
N_{mesh}	33 (31 + 2)	N_{mesh}	70 (61 + 9)
Δz	0.50 cm	Δz	0.25 cm
N_{time}	200	N_{time}	400
Δt	0.0117 min	Δt	0.0088 min
$N_{CFL,max}$	0.47	$N_{CFL,max}$	0.47

plays a central role of connecting the three types of dead volume calculated by MOC.

4 Case studies

A conventional four-zone HPLC SMB laboratory unit for separation of a chiral compound presented elsewhere (Katsuo et al. 2009) was used for the case study. Three cases (Case 1, 2, and 3) were performed, for which Table 2 shows simulation parameters. A linear adsorption equilibrium model was applied to the SMB unit, ignoring mass transfer resistance.

The feed concentration was given at 0.05 g/l of a racemic mixture ($A + B$). 24 shiftings (or 3 rounds) were carried out with a switching time (τ) of 3.5 min. The Peclet numbers ($Pe = v_L L_c / D_{ax}$) of both the adsorptive bed and dead volume were set to be 3000. Linear adsorption isotherms were used for component A (stronger adsorbate) and B (weaker adsorbate):

$$\begin{aligned} n^*_A &= 3.18 C_A \\ n^*_B &= 1.66 C_B \end{aligned} \tag{16}$$

The SMB unit had a 2-2-2-2 bed configuration (8 beds) divided into 4 zones (desorbent, extract, feed and raffinate) for the first case (Case 1) and second case (Case 2), while it had a 2-1-1-2-2 configuration divided into 5 zones for Case 3 where one zone for bed-line flushing was added to increase purity in extract. The flushing flow rate of Case 3 was determined by 105% of bed-line volume. The flushing flow rate is often adjusted by 80–120% of bed-line volume, but that is subordinate to dispersion of a given system.

In Case 1, the dead volume with the bed-head and bed-tail occupied 6.8% (head = 1.1% and tail = 5.7%) of the adsorptive bed volume. Each bed was discretized into 31 spatial mesh points ($N_{mesh} = 31$), the one switching time (τ) was divided into 200 levels ($N_{time} = 200$) and the max-

Table 3 Calculation time comparison with and without dead volume

Dead volume type	CPU time (s)	Overcharge ratio (%)	
		Mesh number[a]	CPU time[b]
No dead volume	5.39		
Case 1 (bed-head and bed-tail)	5.53	6.5	2.6
No dead volume	20.16		
Case 2 (bed-line, 4-zone)	20.26	14.8	0.5
Case 3 (bed-line, 5-zone)	20.29	14.8	0.7

[a] 100×(Mesh number with dead volume—Mesh number without dead volume)/(Mesh number without dead volume)

[b] 100×(CPU time with dead volume—CPU time without dead volume)/(CPU time without dead volume)

imum CFL number was given at 0.47 ($N_{CFL,\max} = 0.47$). The mesh numbers of bed-head and bed-tail ($N_{MOC,head} = 0$ and $N_{MOC,tail} = 2$ for each bed) were obtained from the MOC algorithm described above. Since the bed-head length ($L_{dead,head} = 0.16$ cm) was much less than the spatial stepsize ($\Delta z = 0.5$ cm), the dead volume from the bed-head was not taken into account.

In Cases 2 and 3, the bed-line volume took 4% of the adsorptive bed volume without bed-head and bed-tail. Each bed was discretized into 61 spatial mesh points ($N_{mesh} = 61$), the one switching time (τ) was divided into 400 levels ($N_{time} = 400$) and the maximum CFL number was same as the first case ($N_{CFL,\max} = 0.47$). The grid number of each bed-line ($N_{MOC,bed\text{-}line} = 9$) was 4.5 times greater than that of the first case because of a smaller time stepsize ($\Delta t = 8.75 \times 10^{-3}$ s) and a smaller fluid velocity ($v_{dead,\max} = 3.67$ cm/min) in the desorbent bed-line.

The calculation was performed on a personal computer (2.5 GHz dual-core CPU and 3 GB RAM). If the SMB model including (1) with 6.8% dead volume is solved by using a time integrator as the conventional approaches (Jin and Wankat 2007; Katsuo et al. 2009; Migliorini et al. 1999; Zabka et al. 2008), its computational time would take about 6.8% more than that of the model without dead volume. Indeed, the calculation time of an SMB model with $L_c = 16.02$ cm and $N_{mesh} = 33$ took 6.1% more than that of the model with $L_c = 15$ cm and $N_{mesh} = 31$ in the same CFL number ($N_{CFL,\max} = 0.47$) using the CESE scheme. However, the extended node model with MOC for the dead volume treatment shows more than twice faster performance (overcharge ratio = 2.6%) on the CPU time than the conventional approach, as reported in Table 3. For Cases 2 and 3, the calculation time ratio overcharged by the 4% bed-line dead volume is just 0.5–0.7% (Table 3), even though the total mesh point increases by 15% (from 61 to 70 points). It is due to the fact that only four or five active bed-lines out of eights are solved in the extended node model with MOC, and MOC has a much simpler calculation step than the time integrator used to solve PDEs.

4.1 Case 1 (4-zone SMB with bed-head and bed -tail)

In Fig. 2, liquid concentration profiles are shown within the eight adsorptive beds at three time levels (beginning, middle and last) during the 24th shifting period. The circles (○) and squares (□) are the solutions with dead volume for component A and B respectively, while the bold and thin dashed lines are without dead volume. It is observed that the liquid concentration profiles with dead volume are behind those without dead volume because of time delay caused by the dead volume.

Time lags of concentrations caused by the bed-head and bed-tail are depicted in Fig. 3. As the dead volume of bed-head was ignored and just one mesh point was assigned in all the bed-head (i.e., inlet and exit points are same), time delay is not observed in Fig. 3(a) during the last three switching periods (or over the last three shiftings). Three mesh points were assigned in all the bed-tail, where the first point is the inlet and the third point is the exit of bed-tail. For the 4th bed-tail just before the feeding port, a slight time lag ($t_{lag,tail} = 0.16$ min) is observed between the inlet (○) and exit (×) concentrations in Fig. 3(b). The time lag is accumulated from bed to bed and it affects significantly the internal concentration profiles as shown in Fig. 2.

4.2 Case 2 (4-zone SMB with bed-line)

Figure 4 compares the results with bed-line (○ and □) and without bed-line (bold and thin dashed lines). As the bed-line exists outside the bed, the time delay is not observed in the internal concentration profiles. Instead, the internal concentration of component A (C_A) is lowered because of mass loss from the bed-line ($\dot{m}_{loss,A} = 1.43 \times 10^{-3}$ mg/min). For this complete separation example, the mass conservation of

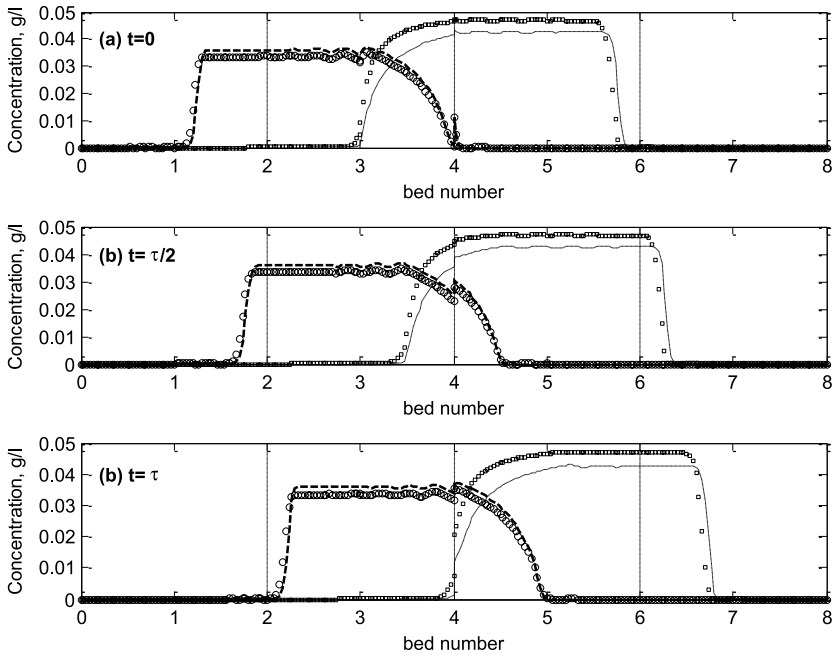

Fig. 2 Liquid concentration distribution over 8 columns at three different times within last shifting time (○: C_A with bed-head and bed-tail, □: C_B with bed-head and bed-tail, — —: C_A without dead volume, and — — —: C_B without dead volume)

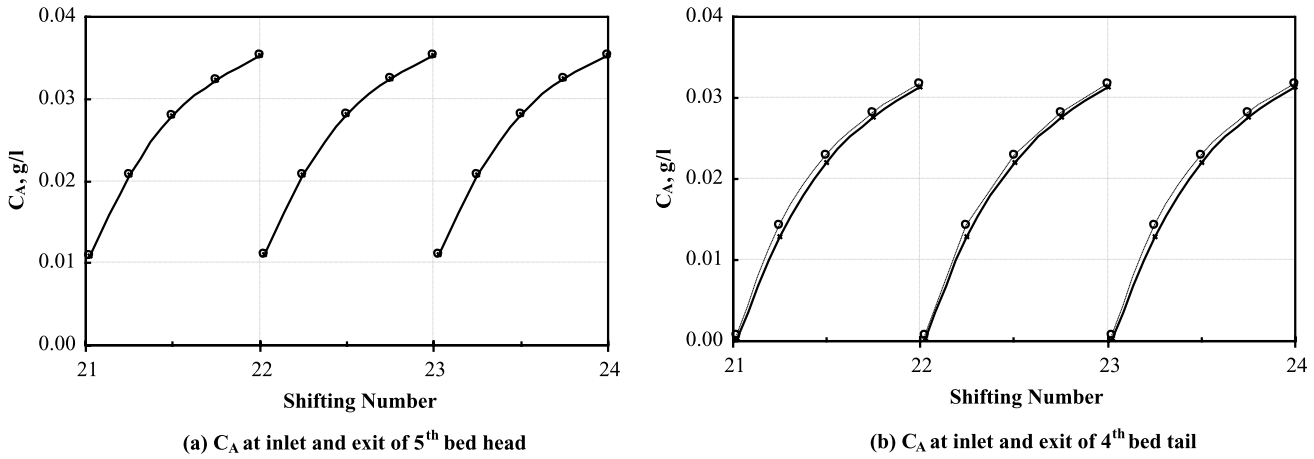

Fig. 3 Time lag of C_A between the inlet and exit of (**a**) bed-head and (**b**) bed-tail (○: inlet concentrations, ×: exit concentrations)

component A is expressed as follows:

$$C_{feed,A} \cdot Q_{feed} = \bar{C}_{ext,A}^{internal} \cdot Q_{ext} + \dot{m}_{loss,A} \tag{17}$$

where $C_{feed,A}$ is the feed concentration of A, $\bar{C}_{ext,A}^{internal}$ is the time-averaged internal extract concentration of A, and Q_{feed} and Q_{ext} are the feed and extract flowrates, respectively. $\bar{C}_{ext,A}^{internal}$ is thus lowered from 0.0255 to 0.0226 g/l by the bed-line. Consequently, the lowered average concentration decreases the recovery of A (R_A):

$$R_A = 100 \times \frac{\bar{C}_{ext,A} \cdot Q_{ext}}{C_{feed,A} \cdot Q_{feed}} \tag{18}$$

where $\bar{C}_{ext,A}$ is the time-averaged extract concentration of A during the last shifting. The fluid trapped in the desorbent bed-line affects little the internal raffinate concentration of component B ($\bar{C}_{raf,B}^{internal}$), because desorbent is a neural component ($\dot{m}_{loss,B} = 0$), as shown in Fig. 4.

Only four of the eight bed-lines are active at any given time in the 4-zone SMB operation with bed-line. The streams trapped in each bed line are withdrawn or injected at the beginning of the second next shifting in the 2-2-2-2 bed configuration. The fluid trapped in the feed bed-line (5th bed-line) will deteriorates, after two shifting times (2τ), the extract purity for the time required to pass through the bed-line. Table 4 shows the extract purity and recovery for the three case studies. As expected, a perfect separation is obtained in Case 1 without bed-line. The purity and recovery decrease in Case 2, because of the bed-line. Therefore, flushing of the extract bed-line is required

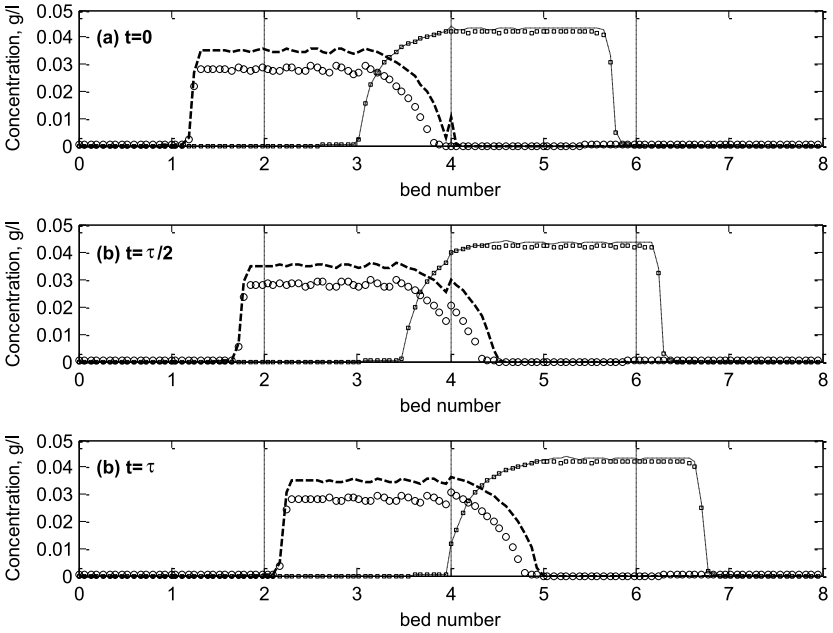

Fig. 4 Liquid concentration distribution over 8 columns at three different times within one shifting time (∘: C_A with bed-line, □: C_B with bed-line, — —: C_A without dead volume, and — — —: C_B without dead volume)

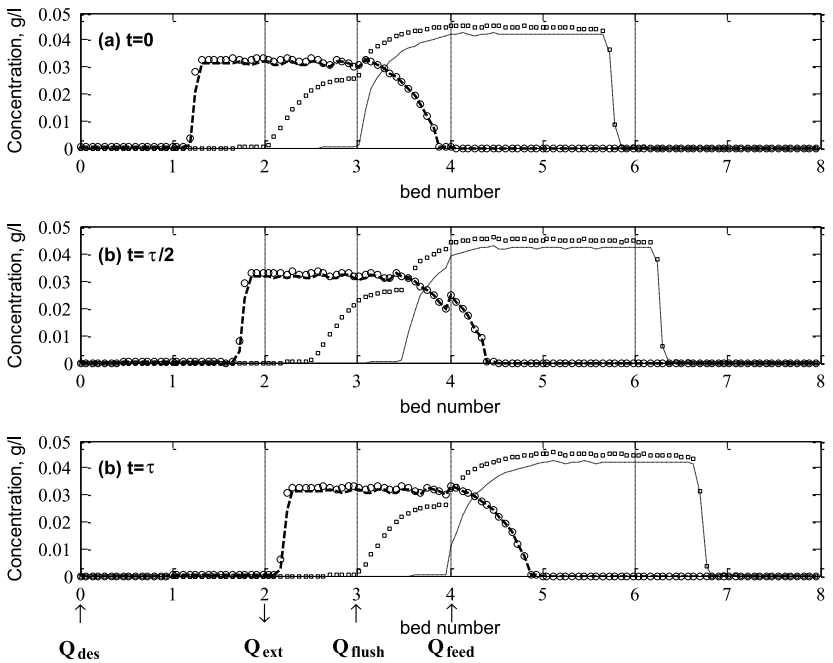

Fig. 5 Liquid concentration distribution over 8 columns at three different times during the last shifting period (∘: C_A in 5-zone, □: C_B in 5-zone, — —: C_A in 4-zone, and — — —: C_B in 4-zone)

Table 4 Comparison of extract purity and recovery for three case studies

Case study	Number of zones	Purity of extract (%)[a]	Recovery (R_A, %)
Case 1	4	100	100
Case 2	4	89.5	99.7
Case 3	5	99.7	99.6[b]

[a] $Purity = 100 \times \frac{\bar{C}_{ext,A}}{\bar{C}_{ext,A}+\bar{C}_{ext,B}}$

[b] $R_A = 100 \times \frac{\bar{C}_{ext,A} \cdot Q_{ext}}{C_{feed,A} \cdot Q_{feed} + C_{flush,A} Q_{flush}}$

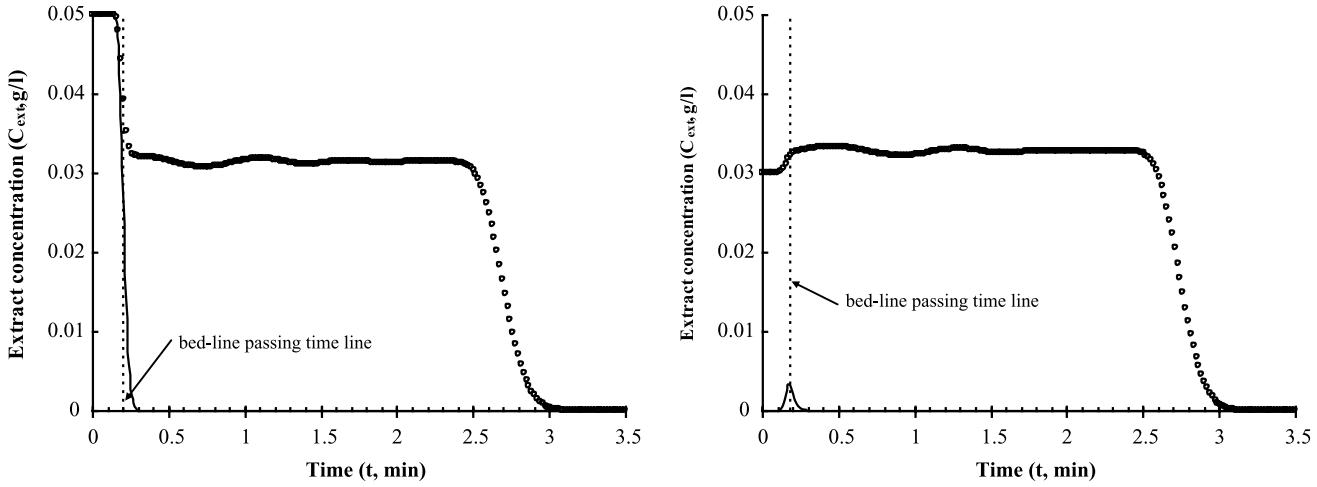

(a) 4-zone operation

(b) 5-zone operation

Fig. 6 Concentration dynamics in extract during the last switching period (○: $C_{ext,A}$, —: $C_{ext,B}$)

to keep the purity high (Minceva and Rodrigues 2003; Wei 1998).

4.3 Case 3 (5-zone SMB with flushing)

For the same bed number as the previous cases, a five-zone operation was performed. The feed mixture trapped in the bed-line was flushed into the third bed by using the pure component A of $C_{flush,A} = 0.03$ g/l. Thus, the bed-line to be used for extract was filled with the pure A in this 5-zone operation. Figure 5 shows liquid concentration evolution at the three different times for Case 2 and Case 3. The tail of concentration B (C_B) is more prolonged and the concentration A (C_A) is slightly more developed in the extract section of Case 3 than those of Case 2, due to the flushing into the third bed. The flushing increases much purity, causing a slight recovery reduction (see Table 4).

In Fig. 6, concentration dynamics are depicted for the four- and five-zone operations during the last shifting period. The feed mixture is withdrawn at the beginning of the switching time from the bed-line in the 4-zone operation. The concentration profiles are dispersed near the fronts because of axial diffusion. In the 5-zone operation, pure component A is collected from the bed-line and a small amount of component B is also eluted around the bed-line passing time. As shown in Fig. 5(a), the prolonged tail of component B caused by the flushing at the third bed affects the extract purity at the beginning of the last switching time.

The purity would be improved by a modification of bed-configuration with the bed number more than eight in the five-zone operation. Since the recovery decreases in increase of dispersion inside dead volume, the flushing flow rate has to be adjusted to maximize the recovery at a given dispersion extent, while satisfying purity requirement. The extended node model incorporated with MOC will be useful to find an optimum flushing flow rate, accurately and efficiently.

5 Conclusions

Dead volumes are always present due to tubes, valves, and pumps in industrial—as well as pilot-scale plants. The extended node model representing realistic port switching of SMB was developed to treat three types of dead volume (bed-head, bed-tail and bed-line) in a unified way based on the method of characteristics (MOC). The non-adsorptive partial differential equation (PDE) describing the dead volume was separated from the adsorptive bed model and was solved by MOC, while the adsorptive PDE bed model was solved by an explicit time integrator (CESE scheme). The MOC approach was constructed to produce a maximum accuracy of the fluid concentration passing through the dead volume at a given CFL (Courant–Friedrichs–Lewy) stability condition.

A standard four-zone SMB with a linear adsorption equilibrium model was used to evaluate performance of the unified approach for the three dead volumes. The bed-head and bed-tail showed time delay of the fluid concentration, while the bed-line affected purity and recovery. A five-zone SMB operation with flushing considerably improved purity in the presence of bed-line. The novel node model solved concentration dynamics caused by the dead volumes (bed-head, bed-tail and bed-line) in a computationally-efficient way.

Acknowledgements We thank Dr. Jinsuk Lee (SamsungTotal, Korea) for helpful discussions about dead volumes in the industrial-scale

SMB process. This work was supported by the Korea Research Foundation Grant funded by the Korean Government (MOEHRD, Basic Research Promotion Fund) (KRF-2008-331-D00108).

References

Andersson, J., Mattiasson, B.: Simulated moving bed technology with a simplified approach for protein purification. J. Chromatogr. A. **1107**(1–2), 88–95 (2006)

Bae, Y.-S., Lee, C.-H.: Partial-discard strategy for obtaining high purity products using simulated moving bed chromatography. J. Chromatogr. A. **1122**(1–2), 161–173 (2006)

Beste, Y.A., Lisso, M., Wozny, G., Arlt, W.: Optimization of simulated moving bed plants with low efficient stationary phases: separation of fructose and glucose. J. Chromatogr. A. **868**(2), 169–188 (2000)

Broughton, D.B., Gerhold, C.G.: Continuous sorption process employing fixed bed of sorbent and moving inlets and outlets. 2 985 589. US Patent (1961)

Bruneau, C.H., Fabrie, P., Rasetarinera, P.: An accurate finite difference scheme for solving convection-dominated diffusion equations. Int. J. Numer. Methods Fluids **24**(2), 169–183 (1997)

Chang, S.C.: The method of space-time conservation element and solution element—a new approach for solving the Navier-Stokes and Euler equations. J. Comput. Phys. **119**(2), 295–324 (1995)

Douglas, J. Jr., Russell, T.F.: Numerical methods for convection-dominated diffusion problems based on combining the method of characteristics with finite element or finite difference procedures. SIAM J. Numer. Anal. **19**(5), 871–885 (1982)

Frey, S.J.: Product recovery from simulated moving bed adsorption. 7 208 651. US Patent (2007)

Gentilini, A., Migliorini, C., Mazzotti, M., Morbidelli, M.: Optimal operation of simulated moving-bed units for non-linear chromatographic separations. II. Bi-Langmuir isotherm. J. Chromatogr. A. **805**(1–2), 37–44 (1998)

Hritzko, B.J., Xie, Y., Wooley, R.J., Wang, N.H.L.: Standing-wave design of tandem SMB for linear multicomponent systems. AIChE J. **48**(12), 2769–2787 (2002)

Jin, W., Wankat, P.C.: Thermal operation of four-zone simulated moving beds. Ind. Eng. Chem. Res. **46**(22), 7208–7220 (2007)

Juza, M., Mazzotti, M., Morbidelli, M.: Simulated moving-bed chromatography and its application to chirotechnology. Trends Biotechnol. **18**(3), 108–118 (2000)

Katsuo, S., Langel, C., Schanen, P., Mazzotti, M.: Extra-column dead volume in simulated moving bed separations: Theory and experiments. J. Chromatogr. A. **1216**(7), 1084–1093 (2009)

Kearney, M.M., Hieb, K.L.: Time variable simulated moving bed process. 5 102 553. US Patent (1992)

Kurup, A.S., Hidajat, K., Ray, A.K.: Optimal operation of an industrial-scale Parex process for the recovery of p-xylene from a mixture of C_8 aromatics. Ind. Eng. Chem. Res. **44**(15), 5703–5714 (2005)

Lim, Y.I.: A nonequilibrium adsorption model satisfying electroneutrality condition for ion-exchange chromatography. Chem. Eng. Commun. **195**(8), 1011–1042 (2008)

Lim, Y.I., Jorgensen, S.B.: A fast and accurate numerical method for solving simulated moving bed (SMB) chromatographic separation problems. Chem. Eng. Sci. **59**(10), 1931–1947 (2004)

Lim, Y.I., Jorgensen, S.B.: Optimization of a six-zone simulated-moving-bed chromatographic process. Ind. Eng. Chem. Res. **46**(11), 3684–3697 (2007)

Lim, Y.I., Chang, S.C., Jorgensen, S.B.: A novel partial differential algebraic equation (PDAE) solver: iterative space-time conservation element/solution element (CE/SE) method. Comput. Chem. Eng. **28**(8), 1309–1324 (2004)

Lim, Y.-I., Lee, J., Bhatia, S.K., Lim, Y.-S., Han, C.: Improvement of para-Xylene SMB process performance on an industrial scale. Ind. Eng. Chem. Res. **49**(7), 3316–3327 (2010)

Ludemann-Hombourger, O., Nicoud, R.M., Bailly, M.: The "VARICOL" process: a new multicolumn continuous chromatographic process. Sep. Sci. Technol. **35**(12), 1829–1862 (2000)

Ludemann-Hombourger, O., Pigorini, G., Nicoud, R.M., Ross, D.S., Terfloth, G.: Application of the "VARICOL" process to the separation of the isomers of the SB-553261 racemate. J. Chromatogr. A. **947**(1), 59–68 (2002)

Ma, Z., Wang, N.H.L.: Standing wave analysis of SMB chromatography: linear systems. AIChE J. **43**(10), 2488–2506 (1997)

Mallmann, T., Burris, B.D., Ma, Z., Wang, N.H.L.: Standing wave design of nonlinear SMB systems for fructose purification. AIChE J. **44**(12), 2628–2646 (1998)

Mattheij, R.M.M., Rienstra, S.W., ten Thije Boonkkamp, J.H.M.: Partial Differential Equations: Modeling, Analysis, Computation. SIAM, Philadelphia (2005)

Mazzotti, M., Storti, G., Morbidelli, M.: Optimal operation of simulated moving bed units for nonlinear chromatographic separations. J. Chromatogr. A. **769**(1), 3–24 (1997)

Migliorini, C., Mazzotti, M., Morbidelli, M.: Simulated moving-bed units with extra-column dead volume. AIChE J. **45**(7), 1411–1420 (1999)

Minceva, M., Rodrigues, A.E.: Influence of the transfer line dead volume on the performance of an industrial scale simulated moving bed for p-xylene separation. Sep. Sci. Technol. **38**(7), 1463–1497 (2003)

Mun, S., Xie, Y., Wang, N.-H.L.: Robust pinched-wave design of a size-exclusion simulated moving-bed process for insulin purification. Ind. Eng. Chem. Res. **42**(13), 3129–3143 (2003)

Nicolaos, A., Muhr, L., Gotteland, P., Nicoud, R.M., Bailly, M.: Application of equilibrium theory to ternary moving bed configurations (four+four, five+four, eight and nine zones), I. Linear case. J. Chromatogr. A. **908**(1–2), 71–86 (2001a)

Nicolaos, A., Muhr, L., Gotteland, P., Nicoud, R.M., Bailly, M.: Application of the equilibrium theory to ternary moving bed configurations (4+4, 5+4, 8 and 9 zones), II. Langmuir case. J. Chromatogr. A. **908**(1–2), 87–109 (2001b)

Noe, R.J.L.: Raffinate line flush in simulated continuous moving bed adsorptive separation process. 5 912 395. US Patent (1999)

Pais, L.S., Loureiro, J.M., Rodrigues, A.E.: Modeling strategies for enantiomers separation by SMB chromatography. AIChE J. **44**(3), 561–569 (1998)

Rajendran, A., Paredes, G., Mazzotti, M.: Simulated moving bed chromatography for the separation of enantiomers. J. Chromatogr. A. **1216**(4), 709–738 (2009)

Sá Gomes, P., Minceva, M., Rodrigues, A.E.: Simulated moving bed technology: old and new. Adsorption **12**(5–6), 375–392 (2006)

Sá Gomes, P., Zabkova, M., Zabka, M., Minceva, M., Rodrigues, A.E.: Separation of chiral mixtures in real SMB units: The FlexSMB-LSRE®. AIChE J. **56**(1), 125–142 (2010)

Schramm, H., Kaspereit, M., Kienle, A., Seidel-Morgenstern, A.: Simulated moving bed process with cyclic modulation of the feed concentration. J. Chromatogr. A. **1006**(1–2), 77–86 (2003)

Seidel-Morgenstern, A., Kessler, L.C., Kaspereit, M.: New developments in simulated moving bed chromatography. Chem. Eng. Technol. **31**(6), 826–837 (2008)

Wang, X., Ching, C.B.: Chiral separation of β-blocker drug (nadolol) by five-zone simulated moving bed chromatography. Chem. Eng. Sci. **60**(5), 1337–1347 (2005)

Wei, C.N.: Multiple grade flush adsorption separation process. 5 750 820. US Patent (1998)

Wooley, R., Ma, Z., Wang, N.H.L.: A nine-zone simulating moving bed for the recovery of glucose and xylose from biomass hydrolyzate. Ind. Eng. Chem. Res. **37**(9), 3699–3709 (1998)

Xie, Y., Chin, C.Y., Phelps, D.S.C., Lee, C.H., Lee, K.B., Mun, S., et al.: A five-zone simulated moving bed for the isolation of six sugars from biomass hydrolyzate. Ind. Eng. Chem. Res. **44**(26), 9904–9920 (2005)

Zabka, M., Minceva, M., Gomes, P.S., Rodrigues, A.E.: Chiral separation of R, S-α-tetralol by simulated moving bed. Sep. Sci. Technol. **43**(4), 727–765 (2008)

Zhang, Z., Mazzotti, M., Morbidelli, M.: Continuous chromatographie processes with a small number of columns: Comparison of Simulated Moving Bed with Varicol, PowerFeed, and ModiCon. Korean J. Chem. Eng. **21**(2), 454–464 (2004a)

Zhang, Z., Morbidelli, M., Mazzotti, M.: Experimental assessment of PowerFeed chromatography. AIChE J. **50**(3), 625–632 (2004b)